
Article:
Nejad, S. and Gladwin, D.T. orcid.org/0000-0001-7195-5435 (2020) Online battery state of power prediction using PRBS and extended Kalman filter. IEEE Transactions on Industrial Electronics, 67 (5). pp. 3747-3755. ISSN 0278-0046

https://doi.org/10.1109/tie.2019.2921280

Online Battery State of Power Prediction Using PRBS and Extended Kalman Filter

S. Nejad, *Member, IEEE*, and D. T. Gladwin

***Abstract*—This paper presents a hybrid battery parametrisation technique for the purpose of battery state-of-charge (SOC) and state-of-power (SOP) monitoring in real time. The proposed technique is centred around an opportunistic initialisation of a dual Extended Kalman Filter (DEKF) algorithm using Pseudo Random Binary Sequence (PRBS) battery excitation. A Second-order electrical equivalent-circuit battery model is used whose parameters are identified using a carefully designed 10-bit 10-Hz PRBS signal while the battery is in a zero- or low-current quiescent mode. The PRBS-identified resistive elements of the battery model are then utilised to provide an initial estimate for the battery's SOP. Once in load conditions, the DEKF algorithm is implemented recursively to provide an accurate estimate of the battery's parameters, SOC and subsequently its SOP in real time. The experimental results obtained form an electrochemical impedance spectroscopy (EIS) method give confidence to the performance of the proposed hybrid battery parametrisation technique.**

***Index Terms*—Battery Excitation; Kalman Filtering; Pseudo Random Binary Sequences**

I. Introduction

BATTERIES are pervasively appearing in more energy storage applications requiring powers ranging from a few watts (e.g. electronic portable devices) to several megawatts (e.g. grid-connected storages). Due to unpredictable load behaviour in such applications, battery management systems (BMSs) are put in place to ensure the battery adheres to a set of time-varying operating constraints, which requires for *in situ* parametrisation of the battery while in load conditions.

Techniques for battery parameterisation can be summarised into three categories of 1) sine-swept methods, e.g. electrochemical impedance spectroscopy (EIS) [1], 2) electrical equivalent-circuit model-based methods, e.g. Kalman filter (KF), recursive least-squares, genetic algorithms or particle swarm optimisation [2]–[4], and 3) electrochemical model-based methods such as nonlinear-coupled partial differential equations (PDEs), where due to the large number of unknowns involved in the latter method, they are often precluded from real-time BMS utilisation [5]. In contrast, due to their effectiveness and simplicity, electrical equivalent-circuit models find themselves in the heart of almost every modern BMS algorithm, where battery states such as state-of-charge (SOC), stat-of-power (SOP), state-of-health (SOH) and state-of-function (SOF) need to be estimated iteratively in real time.

The Kalman filter (KF) algorithm [6] is a robust system identification technique which has been utilised in many battery state estimation problems [7]–[9]. Moreover, the KF can be implemented in either a 'joint' or 'dual' framework to provide a practical solution to simultaneous estimation of both battery states and underlying battery model parameters in real time. Difficulty arises when there is 1) insufficient *a priori* knowledge of the model parameters on initialisation step and/or 2) a lack of persistent excitation in the input signal (e.g. in deep charge/discharge cycles) to properly reveal the battery's dynamic response over a prescribed spectrum. Despite the asymptotic convergence of the KF's covariance matrices towards zero, failing to satisfy the aforementioned pre-conditions often results in a very slow convergence or even divergence in the true battery model parameters [10].

The pseudo random binary sequence (PRBS) is a special type of random signal with properties akin to a band-limited white noise, which can persistently excite the system under test [11]. This particular system identification technique, as opposed to laborious sine-swept methods (e.g. EIS), can provide an elegant solution to online battery impedance characterisation [12], which can serve useful for initialisation of battery models employed in most online BMS applications.

Therefore, this paper proposes a hybrid battery parameterisation technique for the purpose of online battery SOP prediction. The proposed technique is based on PRBS identification of the resistive battery parameters required for SOP prediction, given the battery has been rested for at least 30 minutes prior to load engagement. Upon successful PRBS characterisation, the data is used to statically parametrise a second-order resistor-capacitor (RC) network model and source a nonlinear dual KF algorithm, namely the dual Extended Kalman Filter (DEKF), with a reasonably accurate *a priori* knowledge of the battery model parameters for real-time SOC and SOP estimation under load conditions.

This paper is organised as follows. Section II describes the structure of the battery model used in this paper and provides a steady-state definition for SOP. Section III provides an overview of the DEKF algorithm, presents the formulation of the battery state-space equations, and analyses the DEKF's response to erroneous initialisation conditions. In addition, Section III presents the structure of the proposed hybrid battery identification technique. In Section IV, the theory of PRBS generation is explained. In Section V, the proposed technique is applied to estimate and monitor SOC and SOP of a commercially available 3.6 lithium nickel-manganese-cobalt-

Manuscript received April 30, 2018; revised January 30, 2019; accepted March 17, 2019.

Authors are with the Department of Electronic and Electrical Engineering at the University of Sheffield, United Kingdom. (emails: s.nejad@hotmail.com; d.gladwin@sheffield.ac.uk)

This article has been accepted for publication in a future issue of this journal, but has not been fully edited. Content may change prior to final publication. Citation information: DOI 10.1109/TIE.2019.2921280, IEEE Transactions on Industrial Electronics

oxide (NMC) battery cell under a European Artemis drive cycle. Finally, Section VI concludes this paper.

II. Battery Modelling and Identification

A. Electrical Equivalent-Circuit Model Structure

In this paper, a second-order electrical equivalent-circuit model [13], as show in Fig. 1, is used to describe the transient responses of the battery, where an ideal voltage source is used to represent the battery's open-circuit voltage (OCV) as a function of its SOC, a series resistor, R_s, is used to describe the ohmic losses in the metallic interconnections, and two parallel resistor-capacitor (RC) branches (i.e. $R_1||C_1$ and $R_2||C_2$) are included to capture the long time-constant processes related to diffusional reactions and those short time-constant processes related to charge-transfer and double-layer capacitance phenomena in the battery electrodes [13].

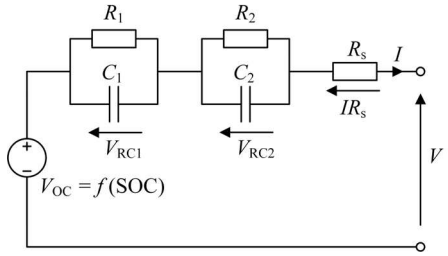

Fig. 1. Second-order equivalent-circuit battery/cell model.

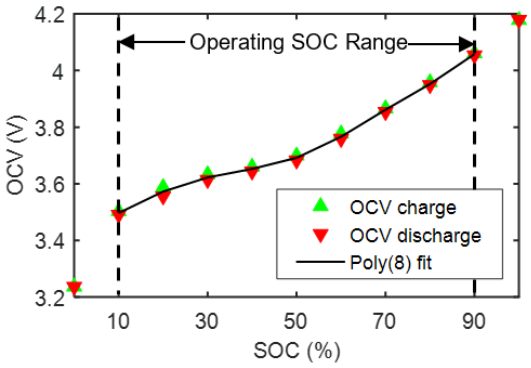

Fig. 2. OCV-SOC relationship for a 3.6 Ah NMC cell, showing an eighth-order polynomial fit over its operational SOC range.

To apply the DEKF algorithm for online battery identification, a pre-defined relationship between the battery's OCV and its SOC is required. For practicality, a battery intended for either motive (e.g. in electric and hybrid-electric vehicles) or stationary (e.g. in grid-tie) applications is operated within a safe SOC envelope, usually between 10-90%. As shown in Fig. 2, within this range, an eighth-order polynomial can be employed to sufficiently describe the average OCV-SOC relationship for the 3.6 Ah lithium-NMC test cell. The polynomial coefficients $a_{0\to8}$ are determined through curve-fitting of the charge and discharge OCV curves, measured as a function of SOC using a pulse-current test profile similar to that reported in [14].

$$V_{OC} = a_8 \times \mathrm{SOC}^8 + \cdots + a_1 \times \mathrm{SOC} + a_0. \tag{1}$$

The coefficients obtained for the lithium-NMC test cell at 25°C are $a_8 = -100.93$, $a_7 = 385.06$, $a_6 = -579.36$, $a_5 = 433.48$, $a_4 = -167.5$, $a_3 = 33.354$, $a_2 = -4.552$, $a_1 = 1.217$, and $a_0 = 3.403$.

B. Impedance-Based SOP Estimation

Equation (2) provides an impedance-based definition for the battery's charge and discharge peak-power capability (i.e. SOP) in the frequency domain,

$$P(\omega) = \begin{cases} \dfrac{V_{\min}(V_{OC} - V_{\min})}{|Z_{bat}(\omega)|} \\ \dfrac{V_{\max}(V_{\max} - V_{OC})}{|Z_{bat}(\omega)|} \end{cases} \tag{2}$$

where $V_{\min}$ is the battery's minimum operating voltage limit, $V_{\max}$ is the maximum voltage threshold, V_{OC} is the battery's OCV as a function of SOC, and $|Z_{bat}(\omega)|$ is the magnitude of the battery's impedance as a function of angular frequency.

Now, to derive a model-based definition for the battery's impedance response, first, a time-domain equation for the RC model of Fig. 1 is formed.

$$V(t) = V_{OC}(\mathrm{SOC}) - [V_{RC1}(t) + V_{RC2}(t)] - [I(t) \cdot R_s] \tag{3}$$

where $V(t)$ is the terminal voltage, $I(t)$ is the throughput current, $I(t) \cdot R_s$ is the series voltage drop, and $V_{RC1}(t)$ and $V_{RC2}(t)$ are the transient voltage drops across $R_1||C_1$ and $R_2||C_2$, respectively.

The model's output equation can be expressed in the Laplace domain as,

$$V(s) = V_{OC} - I(s)\left[R_s + \left(\frac{R_1}{R_1 \cdot sC_1 + 1}\right) + \left(\frac{R_2}{R_2 \cdot sC_2 + 1}\right)\right]. \tag{4}$$

Subsequently, by rearranging (4), the transfer function of the second-order RC battery model can be obtained.

$$Z_{mdl}(s) = \frac{V(s) - V_{OC}}{I(s)} = R_s + \left(\frac{R_1}{R_1 \cdot sC_1 + 1}\right) + \left(\frac{R_2}{R_2 \cdot sC_2 + 1}\right). \tag{5}$$

Under steady-state conditions, as $s \to 0$, the model-based battery impedance described by (5) reduces to,

$$Z_{mdl}^{s\to0} = R_s + R_1 + R_2. \tag{6}$$

Therefore, by substituting $Z_{mdl}^{s\to0}$ into equation (2), the steady-state definitions for discharge and charge SOP in a discrete form can be derived.

$$P_{k+1} = \begin{cases} \dfrac{V_{\min}(V_{OC}(S_k) - V_{\min})}{R_{s,k} + R_{1,k} + R_{2,k}}, & for\ I_k \le 0 \\ \dfrac{V_{\max}(V_{\max} - V_{OC}(S_k))}{R_{s,k} + R_{1,k} + R_{2,k}}, & for\ I_k > 0 \end{cases} \tag{7}$$

From equation (7), it can be deduced that for an accurate and reliable SOP estimate, the DEKF algorithm must be able to produce a convergent estimate for the resistive elements of the RC battery model. Moreover, it is apparent that the battery's OCV also needs to be estimated in real time. To this end, SOC is defined in its discrete-time form using (8) to allow for its inclusion as an estimable state in the DEKF algorithm, which will produce a real-time estimate for the battery's SOC as an input to the polynomial of equation (1) for OCV prediction.

This article has been accepted for publication in a future issue of this journal, but has not been fully edited. Content may change prior to final publication. Citation information: DOI 10.1109/TIE.2019.2921280, IEEE Transactions on Industrial Electronics

$$S_{k+1} = S_k - \frac{\eta \cdot T_s \cdot I_k}{Q_{\text{nom}}} \tag{8}$$

where I_k is the throughput current at discrete-time step k, $Q_{\text{nom}} = 3600 \times C_{\text{nom}}$ and η (for charge $\eta < 1$ and for discharge $\eta = 1$) is the battery's columbic efficiency and C_{nom} is its nominal ampere-hour capacity.

III. DEKF Algorithm

A. Underlying Theory

Generally, a random process to be identified using the DEKF algorithm can be modelled as,

$$\begin{aligned} \mathbf{x}_{k+1} &= f(\mathbf{x}_k, \mathbf{u}_k, \boldsymbol{\theta}_k) + \mathbf{w}_k \\ \mathbf{y}_k &= h(\mathbf{x}_k, \mathbf{u}_k, \boldsymbol{\theta}_k) + \mathbf{v}_k \\ \mathbf{w}_k &\sim N(0, \mathbf{Q}_k^{\text{x}}); \mathbf{v}_k \sim N(0, \mathbf{R}_k^{\text{x}}) \end{aligned} \tag{9}$$

where $\mathbf{x}_k \in \mathbb{R}^n$ is a vector containing the states to be predicted, $\boldsymbol{\theta}_k \in \mathbb{R}^q$ contains the time-varying model parameters, $\mathbf{u}_k \in \mathbb{R}^p$ is the exogenous model input, $\mathbf{y}_k \in \mathbb{R}^m$ is the output and $\mathbf{w}_k \in \mathbb{R}^n$ and $\mathbf{v}_k \in \mathbb{R}^m$ are the zero-mean process and measurement noises of covariance $\mathbf{Q}_k^{\text{x}}$ and $\mathbf{R}_k^{\text{x}}$ respectively. The nonlinear function $\boldsymbol{f}(\cdot)$ relates the states estimated at discrete time k-1 to those at the current time step k, and $\boldsymbol{h}(\cdot)$ maps the updated states to the measurements taken at time step k.

Assuming the model parameters vary slowly over time (i.e. minutes to hours), a second EKF can be designed to adaptively estimate R_s, R_1, C_1, R_2 and C_2.

$$\begin{aligned} \boldsymbol{\theta}_{k+1} &= \boldsymbol{\theta}_k + \mathbf{r}_k \\ \mathbf{d}_k &= h(\mathbf{x}_k, \mathbf{u}_k, \boldsymbol{\theta}_k) + \mathbf{e}_k \\ \mathbf{r}_k &\sim N(0, \mathbf{Q}_k^{\theta}); \mathbf{e}_k \sim N(0, \mathbf{R}_k^{\theta}) \end{aligned} \tag{10}$$

where the dynamics of changes in parameters vector $\boldsymbol{\theta}_k$ are attributed to a small "imaginary" white noise $\mathbf{r}_k \in \mathbb{R}^p$ of covariance $\mathbf{Q}_k^{\theta}$ that evolves the parameters over time. The output equation $\mathbf{d}_k \in \mathbb{R}^m$ is given as a measurable function of $\boldsymbol{\theta}_k$ and a white noise $\mathbf{e}_k \in \mathbb{R}^m$ of covariance $\mathbf{R}_k^{\theta}$ to account for the measurement uncertainties. For more details on DEKF update equations, the reader is referred to [13].

B. Formulation of Battery State-Space Equations

The state-space equations representing the RC model of Fig. 1 can be expressed by,

$$\begin{aligned} \boldsymbol{f}(\cdot) &= \begin{bmatrix} \text{SOC}_{k+1} \\ V_{\text{RC1}_{k+1}} \\ V_{\text{RC2}_{k+1}} \end{bmatrix} = \begin{bmatrix} 1 & 0 & 0 \\ 0 & e^{\frac{-T_s}{\tau_1}} & 0 \\ 0 & 0 & e^{\frac{-T_s}{\tau_2}} \end{bmatrix} \begin{bmatrix} \text{SOC}_k \\ V_{\text{RC1}_k} \\ V_{\text{RC2}_k} \end{bmatrix} + \\ & \begin{bmatrix} -\frac{\eta T_s}{Q_{\text{nom}}} & 0 & 0 \\ 0 & R_1\left(1 - e^{\frac{-T_s}{\tau_1}}\right) & 0 \\ 0 & 0 & R_2\left(1 - e^{\frac{-T_s}{\tau_2}}\right) \end{bmatrix} I_k \\ \boldsymbol{\theta}_k &= [R_s, R_1, \tau_1, R_2, \tau_2]^{\text{T}} \\ \boldsymbol{h}(\cdot) &= V_k = V_{\text{OC}}(\text{SOC}_k) - V_{\text{RC1}_k} - V_{\text{RC2}_k} - I_k R_s \end{aligned} \tag{11}$$

where $\tau_1 = R_1 C_1$ and $\tau_2 = R_2 C_2$. Finally, the Jacobian matrices required for DEKF's update steps are given in (12) and (13).

$$\mathbf{F}_{k-1} = \left.\frac{\partial \boldsymbol{f}(\cdot)}{\partial \mathbf{x}_k}\right|_{\mathbf{x}_k = \hat{\mathbf{x}}_{k-1}^+} = \begin{bmatrix} 1 & 0 & 0 \\ 0 & e^{\frac{-\Delta t}{\tau_1}} & 0 \\ 0 & 0 & e^{\frac{-\Delta t}{\tau_2}} \end{bmatrix} \tag{12}$$

$$\left.\begin{aligned} \mathbf{H}_k^{\theta} &= \left.\frac{\text{d}\boldsymbol{h}(\cdot)}{\text{d}\boldsymbol{\theta}_k}\right|_{\boldsymbol{\theta}_k = \hat{\boldsymbol{\theta}}_k^-} = \frac{\partial \boldsymbol{h}(\cdot)}{\partial \hat{\boldsymbol{\theta}}_k^-} + \frac{\partial \boldsymbol{h}(\cdot)}{\partial \hat{\mathbf{x}}_k^-} \cdot \frac{\text{d}\hat{\mathbf{x}}_k^-}{\text{d}\hat{\boldsymbol{\theta}}_k^-} \\ \frac{\text{d}\hat{\mathbf{x}}_k^-}{\text{d}\hat{\boldsymbol{\theta}}_k^-} &= \frac{\partial \boldsymbol{f}(\cdot)}{\partial \hat{\boldsymbol{\theta}}_k^-} + \frac{\partial \boldsymbol{f}(\cdot)}{\partial \hat{\mathbf{x}}_{k-1}^+} \cdot \frac{\text{d}\hat{\mathbf{x}}_{k-1}^+}{\text{d}\hat{\boldsymbol{\theta}}_k^-} \\ \frac{\partial \boldsymbol{h}(\cdot)}{\partial \hat{\boldsymbol{\theta}}_k^-} &= [-I_{k-1} \quad 0 \quad 0 \quad 0 \quad 0] \\ \frac{\text{d}\hat{\mathbf{x}}_k^-}{\text{d}\hat{\boldsymbol{\theta}}_k^-} &= \begin{bmatrix} 0 & 0 & 0 & 0 & 0 \\ 0 & a_{2,2} & a_{2,3} & 0 & 0 \\ 0 & 0 & 0 & a_{3,4} & a_{3,5} \end{bmatrix} \end{aligned}\right\} \tag{13}$$

where,

$a_{2,2} = -I_{k-1} \cdot (\exp(\Delta t/\tau_1^2) - 1)$;
$a_{2,3} = (\Delta t/\tau_1^2) \cdot \left(\hat{x}_{2,k}^- - R_1 I_{k-1}\right) \exp(-\Delta t/\tau_1)$;
$a_{3,4} = -I_{k-1} \cdot (\exp(\Delta t/\tau_2^2) - 1)$; and
$a_{3,5} = (\Delta t/\tau_2^2) \cdot \left(\hat{x}_{3,k}^- - R_2 I_{k-1}\right) \exp(-\Delta t/\tau_2)$.

C. DEKF Response to Unknown Initial Conditions

To gain a better understanding of the DEKF's performance under unknown initial conditions, a dynamic experiment is devised and implemented on the NMC test cell. The load profile used here is an Artemis-based drive cycle [15], which is commonly used in verification of new BMS algorithms for electric vehicle applications in Europe. The complete test profile starts with a standard charge/discharge cycle to initialise the coulomb-counter used for the calculation of a reference SOC for comparison purposes, followed by 28 consecutive Artemis-based drive cycles of Fig. 3, in order to dynamically discharge the test cell from 80% to 20% SOC.

TABLE II
INITIAL RC MODEL PARAMETERS FOR DEKF BATTERY IDENTIFICATION

Parameters	R_s(mΩ)	R_1(mΩ)	C_1(F)	R_2(mΩ)	C_2(F)
Datasheet	20	10	1000	10	100
EIS-attained	26.95	12.6	1853	3.2	17.08

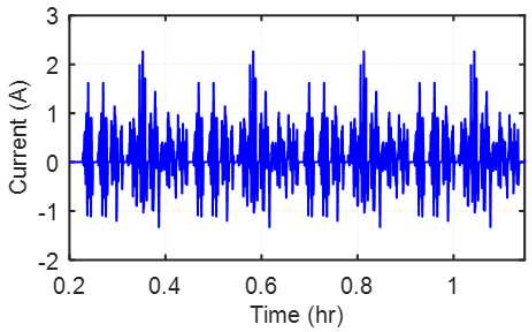

Fig. 3. The current profile used for dynamic excitation of the NMC test cell, showing a single repetition of the Artemis-based drive cycle.

In the following sub-sections, the DEKF's performance capability in terms of voltage, SOC and parameter estimation errors is explored for two cases; 1) DEKF initialised with best-guess RC model parameters taken from the cell datasheet, and, 2) DEKF initialised with *a priori* knowledge of the model parameters that were obtained through curve-fitting of the complex battery impedance data at 25°C and 80% SOC using the EIS method [16]. The EIS test was performed using a Solartron 1260 electrochemical interface in conjunction with a Solartron 1287 frequency response analyser, over the frequency range of 5 mHz up to 5 kHz, at a resolution of 15 steps per decade. The amplitude of the excitation signal was chosen at 5 mV, low enough to avoid nonlinearities due to charge modification, but high enough for good noise immunity. The test cell's SOC was adjusted by using a 0.5C constant-current pulse followed by a zero-current relaxation period of 1 hour to ensure the cell has reached an equilibrium state prior to conducting the EIS. For more details on the EIS testing procedure adopted herein, the reader is referred to [17].

Table II provides the RC model parameters for the two filter initialisation scenarios. It should be noted that for both cases, the initial SOC is intentionally set to 20% instead of true 79.12%. This is to demonstrate the robustness of the DEKF for SOC estimation, even under erroneous initialisation of the battery model parameters. The state and weight filters in the DEKF algorithm are initialised according to (14).

$$\begin{gathered}\mathbf{x}_0 = \begin{bmatrix} \mathrm{SOC}_0 \\ V_{\mathrm{RC1},0} \\ V_{\mathrm{RC2},0} \end{bmatrix} = \begin{bmatrix} 0.2 \\ 0 \\ 0 \end{bmatrix};\ \boldsymbol{\theta}_0 = [R_s, R_1, \tau_1, R_2, \tau_2]^{\mathrm{T}} \\ \mathbf{Q}_0^{\mathrm{x}} = \mathrm{diag}_n\{1\times 10^{-8}\};\ \mathbf{P}_{\tilde{\mathrm{x}},0}^{+} = \mathrm{diag}_n\{10\}; \\ \mathbf{R}_0^{\mathrm{x}} = \mathrm{diag}_m\{0.1\} \\ \mathbf{Q}_0^{\theta} = \mathrm{diag}_q\{1\times 10^{-12}\};\ \mathbf{P}_{\tilde{\theta},0}^{+} = \mathrm{diag}_q\{10\}; \\ \mathbf{R}_0^{\theta} = \mathrm{diag}_m\{10\}\end{gathered} \tag{14}$$

where diag{·} is a diagonal matrix of size $n = 3$, $m = 1$, and $q = 5$. Note that the error covariance matrices $\mathbf{P}_{\tilde{\mathrm{x}},0}^{+}$ and $\mathbf{P}_{\tilde{\theta},0}^{+}$ are set to a large value at initialisation to account for any uncertainties in both state and weight filters' initial conditions. However, for the EIS-obtained parameters, since the weight EKF is initialised with *a prior* knowledge, the initial error covariance is set to a small value, i.e. $\mathbf{P}_{\tilde{\theta},0}^{+} = \mathrm{diag}_5\{0.01\}$.

1) Voltage Estimation Response

Table III presents the voltage RMSE values calculated for the DEKF algorithm initialised with the aforementioned model parameters. Note that the RMSE has been calculated from the time that voltage estimate satisfied a 5% error bound with respect to the measured signal. This ensured that large errors in the model states during the convergence phase did not skew the results. From the presented RMSE results, it can be said that, the DEKF algorithm's performance in battery terminal voltage estimation is not significantly improved by correctly initialising the battery model parameters.

2) SOC Estimation Response

Similarly, the SOC estimates obtained for the two filter initialisation scenarios were plotted on the same graph, as presented in Fig. 4. Despite the large errors in the initial SOC sate and the battery model parameters, the state EKF delivers a satisfactory performance by converging to the actual SOC within the first 15 minutes of filter initialisation. This is owed to the fairly accurate OCV-SOC relationship that was empirically derived for the test cell using the eighth-order polynomial function given in equation (1).

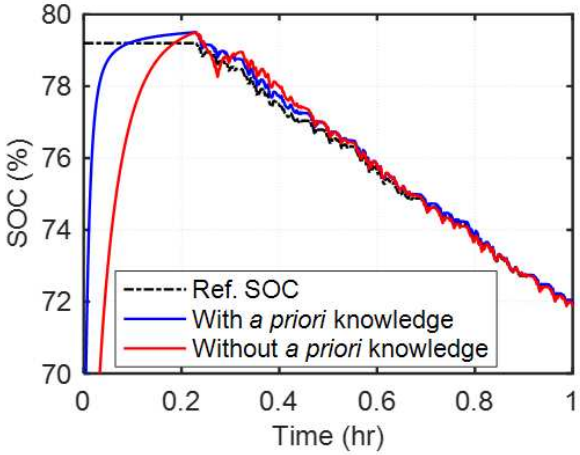

Fig. 4. The SOC estimation performance of the DEKF algorithm with respect to correct and erroeneous initial model parameters.

TABLE III
VOLTAGE ESTIMATION PERFORMANCE OF THE DEKF ESTIMATOR

Initial condition	RMSE Voltage (mV)
Without *a priori* knowledge of RC parameters	1.7e-3
With *a priori* knowledge of RC parameters	8.9e-4

TABLE IV
SOC ESTIMATION PERFORMANCE OF THE DEKF ESTIMATOR

Initial condition	RMSE SOC (%)
Without *a priori* knowledge of RC parameters	0.8
With *a priori* knowledge of RC parameters	0.49

Table IV presents the RMSE SOC values calculated from the moment that the 5% error-bound criterion has been met. Evidently, under both scenarios, the state filter produces a SOC estimate with less than ±1% error. This outcome demonstrates the robustness of the DEKF estimator regardless of the accuracy of the initial model parameters.

3) Battery Parameter Identification Performance

Fig. 5 compares the parameter estimation capability of the DEKF algorithm for both correct and incorrect initial conditions. It is evident that, despite its excellent SOC estimation performance, the DEKF is significantly affected by the slow time-variability of the battery model parameters, which can have a detrimental effect on the performance of the DEKF algorithm. Therefore, by having *a priori* knowledge of the battery parameters at the initialisation step, it is possible to achieve a more realistic estimate for the battery's RC model parameters, which is key to reliable BMS operation.

This article has been accepted for publication in a future issue of this journal, but has not been fully edited. Content may change prior to final publication. Citation information: DOI 10.1109/TIE.2019.2921280, IEEE Transactions on Industrial Electronics

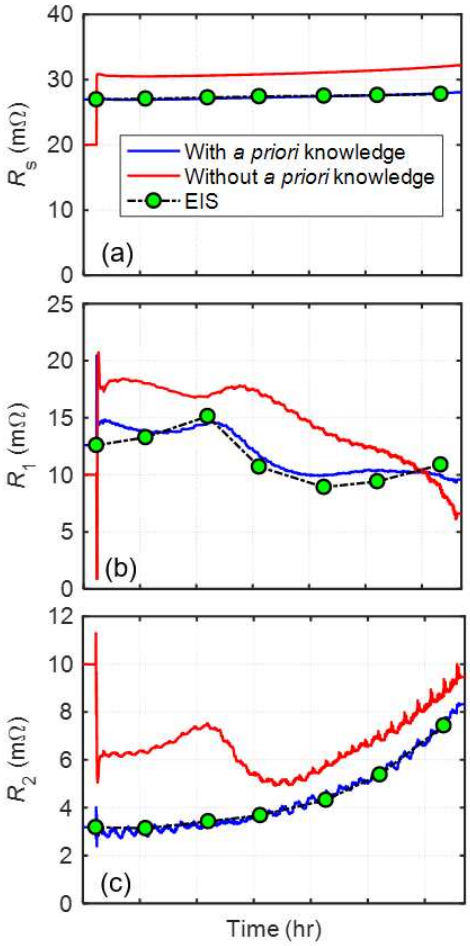

Fig. 5. Comparison of identified resistive-element parameters with and without *a priori* knowledge at SOC = 80% and EIS-identified values.

D. Proposed Hybrid Battery Identification Technique

The structure of the proposed hybrid battery identification technique is presented in Fig. 6. The PRBS excitation is conducted while the battery is in the rest mode (i.e. quiescent or very low-current mode). Once in the active mode (i.e. under load conditions), the DEKF is initialised with the PRBS-attained RC model parameters, which is then ran recursively to yield an adaptive estimate for R_s, R_1, and R_2 in real time. In order to ensure a steady-state condition prior to PRBS excitation, the test cell is allowed to relax for 30 minutes. This relaxation period ensures the battery has reached an electrochemical and thermodynamic equilibrium, a requirement for better PRBS identification.

According to control theory, the observability of a linear system can be determined if matrix O_b has full rank. This is applied to the linearised system.

$$O_b = \begin{bmatrix} \boldsymbol{C} \\ \boldsymbol{CA} \\ \boldsymbol{CA}^2 \\ \vdots \\ \boldsymbol{CA}^{n-1} \end{bmatrix} \tag{15}$$

where, $\boldsymbol{C} = [\partial OCV/\partial SOC \quad -1 \quad -1]$; and $\boldsymbol{A} = \boldsymbol{F}_{k-1}$. In this case, by providing the state filter (where $n = 3$) with an accurate set of battery parameters obtained from the proposed PRBS identification technique, and providing an initial estimate for SOC by reading the battery's OCV after a 30-minute relaxation period, the system in hand may be deemed observable. However, without a sufficient knowledge of the battery parameters to construct the $\boldsymbol{A}$ matrix at DEKF initialisation, observability, and thus, the convergence of the battery states cannot be guaranteed.

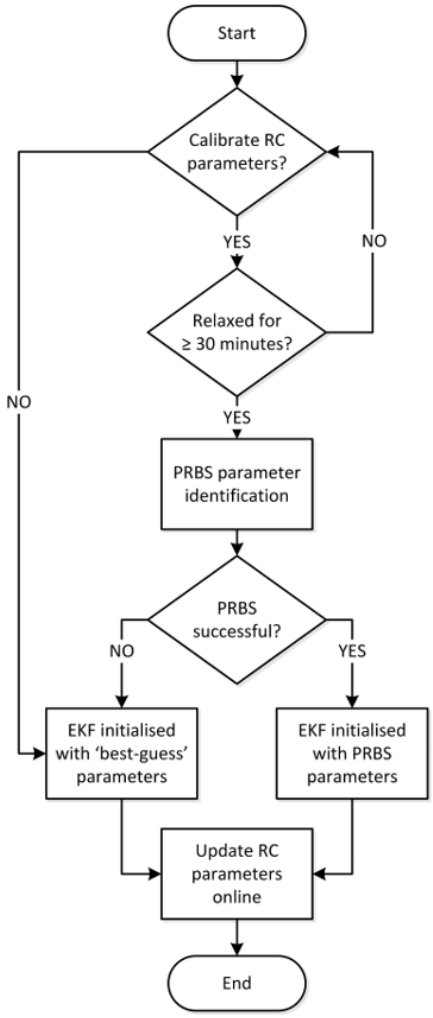

Fig. 6. Block diagram demonstrating the concept of the proposed hybrid battery parameter identification.

Upon the completion of PRBS excitation, the battery model parameters are identified using the nonlinear Levenberg-Marquardt algorithm [18], whereby minimisation of (16), parameters vector, $\boldsymbol{\theta_k}$, in (11) are accurately initialised. In case the PRBS excitation procedure is interrupted due unpredictable consumer behaviour, the parameters vector of the weight EKF is provided with 'best-guess' values at the time of initialisation.

$$|\epsilon|^2 = \left(\ln|Z_{\text{prbs}}(\omega)| - \ln|Z_{\text{mdl}}(\omega)|\right)^2 + \left(\phi_{\text{prbs}}(\omega) - \phi_{\text{mdl}}(\omega)\right)^2 \tag{16}$$

where $|Z_{\text{prbs}}(\omega)|$ is the magnitude and $\phi_{\text{prbs}}(\omega)$ is the resulting phase angle of the battery's frequency response under PRBS excitation, and $|Z_{\text{mdl}}(\omega)|$ and $\phi_{\text{mdl}}(\omega)$ are the magnitude and phase angle of the RC model's frequency response, all as functions of angular frequency.

IV. PRBS Generation for DEKF Initialisation

A typical PRBS sequence is comprised of binary 'zeros' and 'ones' that are switched according to a pre-determined pattern [19]. The most commonly-used PRBS's are those based on maximum-length sequences. They can be both generated in hardware or software, using a number of linear-feedback shift registers (LFSR) with modulo-two (XOR) feedback taken from some pre-determined tap positions [19].

When designing a PRBS signal, there are two base parameters that must be carefully selected. These are the source clock frequency (f_{clk}) and the number of shift registers (n), which in turn define the PRBS frequency bandwidth and the test duration. For a maximum-length PRBS, the test duration is given by (17) where $N = 2^n - 1$ is sequence length.

$$T_{\text{prbs}} = \frac{N}{f_{\text{clk}}} \tag{17}$$

In [20] and [21] the authors have shown that by analysing the signal power spectral density (PSD), the bandwidth over which the PRBS data is useable can be established as,

$$f_{\text{min}} = f_{\text{clk}}/N\,;\; f_{\text{max}} = \frac{f_{\text{clk}}}{2.3};$$
$$f_{\text{band}} = f_{\text{clk}}\left(\frac{1}{2.25} - \frac{1}{N}\right);\; f_{\text{norm}} = \frac{f_{\text{band}}}{f_{\text{max}}} = 1 - \frac{2.25}{N}. \tag{18}$$

where f_{band} is the theoretical frequency band and f_{norm} is the normalised frequency band over which the PRBS information are useful.

In [12], the authors have shown that f_{norm} increases exponentially with increasing PRBS bit-length, n. However, the resulting increase in test duration becomes disadvantageous. It follows that there exists a trade-off at $n = 10$, leading to a PRBS perturbation signal that is less than two minutes long (i.e. 102 seconds) and covers a theoretical band of $0.01\text{ Hz} \leq f \leq 4.44\text{ Hz}$. Note that for a 10-bit PRBS, *XOR* feedback must be taken from the seventh and the tenth shift registers [19].

Finally, to compute the complex impedance of the battery system, a conversion of the signals in time-domain to frequency-domain is required. This is often realised by taking the discrete Fourier transform of the acquired input/out data [22]. This operation is described by,

$$Z_{\text{prbs},k}(f) = \frac{\mathcal{F}\{V_k\}}{\mathcal{F}\{I_k\}};\; f = k\frac{f_s}{n_s};\; n_{\text{s}} = N\left(\frac{f_{\text{s}}}{f_{\text{clk}}}\right);\quad \forall\, k \leq n_s - 1 \tag{19}$$

where $\mathcal{F}\{\cdot\}$ denotes the Fourier transform, $f_{\text{s}} = 100$ Hz is the sampling rate and n_{s} is the number of samples.

V. Experimental Verification

In order to verify the performance of the proposed hybrid PRBS-DEKF battery identification technique for online SOP estimation, a test profile is devised (see Fig. 7) and implemented using the experimental setup described in [16]. The test profile consists of a standard HPPC repetition [23], followed by a 10-bit 10-Hz PRBS signal. This test is applied over the SOC range of 10-90%.

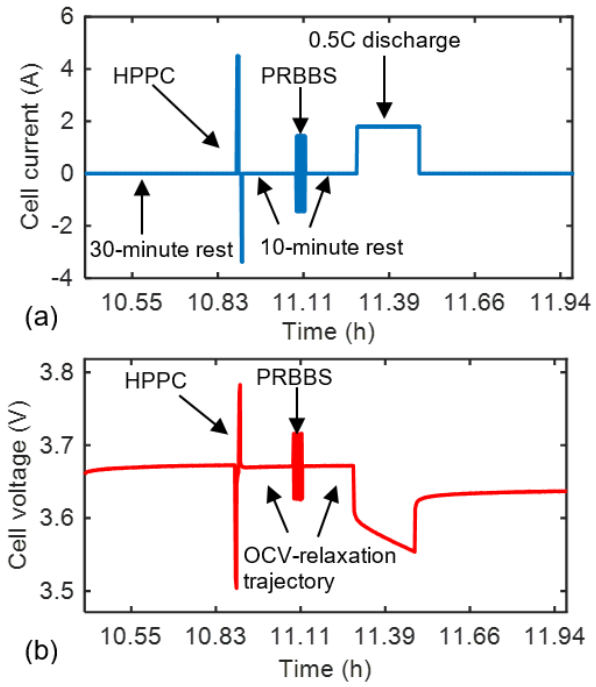

Fig. 7. Excerpt of the modified HPPC test profile with PRBS, showing (a) current and (b) voltage waveforms.

Fig. 8 presents the RC model parameters identified as a function of SOC at 25°C, using the EIS, PRBS and the proposed hybrid DEKF methods. It should be noted that in the latter case, the SOC state has been allowed to fully converge (i.e. enter and stay within ±5% error band), before the first set of estimated parameters were used for absolute error calculations; thus, the results for the hybrid DEKF estimator are displayed over the SOC range of 70% to 20%.

The performance of each technique is quantified by calculating the mean-absolute-error (MAE) between the PRBS- and DEKF-identified model parameters with those obtained from the fairly accurate EIS method.

$$\text{MAE}\ (\%) = \left(\frac{1}{d}\sum_{i=1}^{d}\frac{|\hat{\rho}_i - \rho_i|}{\rho_i}\right) \times 100 \tag{20}$$

where $\hat{\rho}_i$ is the estimated model parameter using the PRBS or hybrid DEKF method, ρ_i is the EIS-identified parameter and d is the number of SOC steps at which the test is conducted. Table V presents the resulting MAEs and it is evident that the low-cost PRBS technique is capable of producing a fairly accurate set of model parameters at each SOC step. Moreover, by accurately initialising the DEKF algorithm with PRBS-identified parameters at 80% SOC, the MAE is even further reduced while operating in load condition.

TABLE V
Statistical Assessment of The Proposed PRBS and Hybrid DEKF Identification Methods

Identification method	MAE (%)				
	R_s	R_1	C_1	R_2	C_2
PRBS	0.387	10.42	13.20	14.36	24.03
Hybrid dual-EKF	0.129	4.09	12.35	4.76	21.68

This article has been accepted for publication in a future issue of this journal, but has not been fully edited. Content may change prior to final publication. Citation information: DOI 10.1109/TIE.2019.2921280, IEEE Transactions on Industrial Electronics

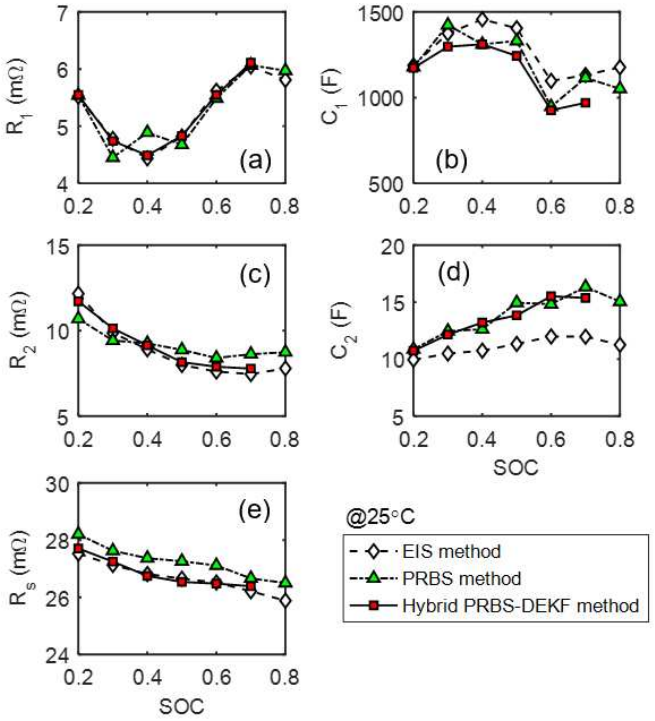

Fig. 8. Comparison of RC model parameters identified using EIS, PRBS and the proposed hybrid DEKF method at 25°C.

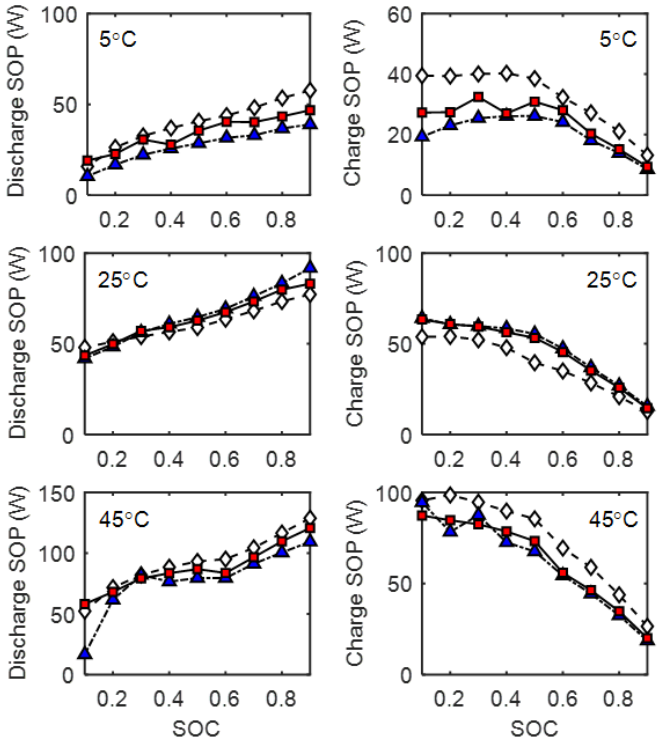

Fig. 9. Comparison of SOP estimates obtained using the HPPC (white diamonds), EIS (blue triangles) and PRBS (red squares) methods.

The test cell was applied with the profile of Fig. 7 at three controlled temperature settings of 5°C, 25°C and 45°C, over 10-90% SOC range. The resulting RC parameters identified using the HPPC method, EIS method and the 10-bit 10-Hz PRBS signal designed in this paper were then used in equation (7) to characterise the battery's charge and discharge SOP at every 10% SOC step. As presented in Fig. 9, the PRBS method is capable of producing a reliable and comparable SOP estimate over a wide range of operating temperatures.

In general, the accuracy of SOP estimate obtained using (7) depends on the quality of $\hat{R}_s$, $\hat{R}_1$, $\hat{R}_2$ and $\hat{V}_{OC}$ estimates. In Fig. 5, it was shown that, if initialised with correct battery model parameters at time-step $k = 0$, the DEKF estimator can robustly track any deviations in the model parameters caused by operating conditions. Thus, a PRBS-initialised DEKF estimator is designed (see Fig. 10) to produce an adaptive SOP estimate in real time. The proposed algorithm is based on the hybrid DEKF battery identification technique developed in this paper, starting with PRBS initialisation of the parameters vector ($\boldsymbol{\theta}_k$) in (11). Thereafter, $\hat{R}_s$, $\hat{R}_1$ and $\hat{R}_2$ are estimated by the DEKF at each time-step k and $\hat{V}_{OC}$ is predicted based on the DEKF-estimated SOC using the polynomial given by (1). The dynamic performance of the proposed DEKF-based SOP estimator is verified using the Artemis-based load profile of Fig. 3.

Fig. 11 compares the online SOP estimates obtained using the PRBS-initialised DEKF estimator and the HPPC method. It can be seen that, as the battery is discharged from 80% SOC down towards 20%, the DEKF-estimated discharge SOP poses a decreasing trend, while the charge SOP estimate shows the opposite. This is an expected behaviour caused by the battery's charge acceptance/retention at its either SOC extremes [24], which is further verified against the HPPC results, where a similar trend in the predicted powers can be observed.

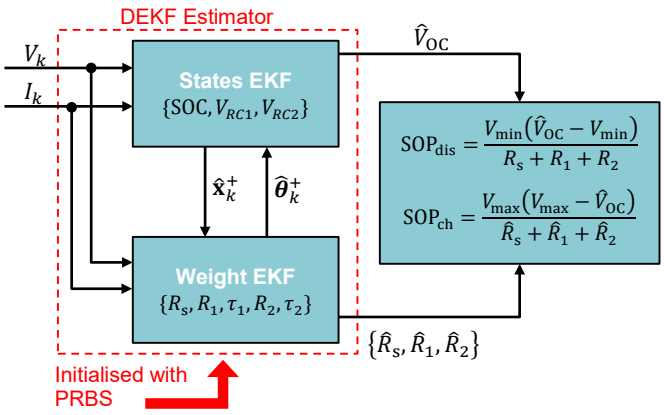

Fig. 10. Block diagram of the proposed online battery SOP estimator.

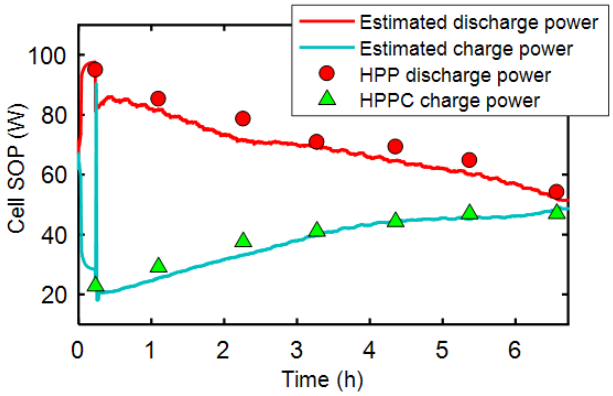

Fig. 11. Comparison of the online SOP estimates obtained using the PRBS-initialised DEKF estimator and the HPPC method.

At SOC = 70%, the cell's DEKF-estimated discharge and charge SOPs are, respectively, 82 W and 25 W, whilst for the

HPPC method, the test cell's SOP is estimated at 85 W and 29 W for discharge and charge respectively. Similarly, at the lower end of SOC range, the DEFK-estimated cell power is 52 W and 49 W, whilst the HPPC-predicted power levels are 54 W and 47 W for discharge and charge respectively. Despite the fact that HPPC and the proposed battery SOP estimation techniques differ in implementation, a good agreement between the powers estimated can be observed.

VI. Conclusion

For a reliable BMS operation, the incorporated battery model needs to be identified accurately in real time; to this end, the DEKF algorithm has been extensively applied in many online battery identification problems. However, for an accurate identification of the battery model parameters using the DEKF algorithm, the filter must be initialised with sufficient a priori knowledge of the unknown parameters. In practice, such information might not be available to the BMS, or the input signal may not be persistently exciting at all times for convergence to occur. Thus, in this paper, a hybrid PRBS-DEKF battery identification technique has been put forward to adaptively identify the parameters of a second-order RC equivalent-circuit battery model. The technique involves PRBS characterisation of the battery/cell to provide the DEKF algorithm with an accurate set of initial battery model parameters prior to load engagement. The accuracy of the RC parameters identified by the PRBS and the hybrid PRBS-DEKF methods were experimentally verified against the well-established EIS battery identification method. For completeness, the performance of the proposed PRBS and the hybrid DEKF algorithm were both tested for online SOP prediction of a 3.6 Ah lithium-NMC cell.

References

[1] Q.-K. Wang, Y.-J. He, J.-N. Shen, X. Hu, and Z.-F. Ma, "State of Charge-Dependent Polynomial Equivalent Circuit Modeling for Electrochemical Impedance Spectroscopy of Lithium-ion Batteries," *IEEE Trans. Power Electron.*, 2017.

[2] Z. Yu, L. Xiao, H. Li, X. Zhu, and R. Huai, "Model Parameter Identification for Lithium Batteries Using the Coevolutionary Particle Swarm Optimization Method," *IEEE Trans. Ind. Electron.*, vol. 64, no. 7, pp. 5690–5700, 2017.

[3] Z. Wang, J. Ma, and L. Zhang, "State-of-Health Estimation for Lithium-Ion Batteries Based on the Multi-Island Genetic Algorithm and the Gaussian Process Regression," *IEEE Access*, vol. 5, pp. 21286–21295, 2017.

[4] H. Rahimi-Eichi, F. Baronti, and M.-Y. Chow, "Online Adaptive Parameter Identification and State-of-Charge Coestimation for Lithium-Polymer Battery Cells," *Ind. Electron. IEEE Trans.*, vol. 61, no. 4, pp. 2053–2061, Apr. 2014.

[5] G. Fan, X. Li, and M. Canova, "A Reduced-Order Electrochemical Model of Li-Ion Batteries for Control and Estimation Applications," *IEEE Trans. Veh. Technol.*, vol. 67, no. 1, pp. 76–91, 2018.

[6] R. E. Kalman, "A new approach to linear filtering and prediction problems," *J. basic Eng.*, vol. 82, no. 1, pp. 35–45, 1960.

[7] S. Peng, C. Chen, H. Shi, and Z. Yao, "State of charge estimation of battery energy storage systems based on adaptive unscented Kalman filter with a noise statistics estimator," *IEEE Access*, vol. 5, pp. 13202–13212, 2017.

[8] Q. Yu, R. Xiong, C. Lin, W. Shen, and J. Deng, "Lithium-ion battery parameters and state-of-charge joint estimation based on H-infinity and unscented Kalman filters," *IEEE Trans. Veh. Technol.*, vol. 66, no. 10, pp. 8693–8701, 2017.

[9] K.-T. Lee, M.-J. Dai, and C.-C. Chuang, "Temperature-compensated model for lithium-ion polymer batteries with extended kalman filter state-of-charge estimation for an implantable charger," *IEEE Trans. Ind. Electron.*, vol. 65, no. 1, pp. 589–596, 2018.

[10] V. V Chalam, *Adaptive Control Systems: Techniques and Applications*. New York: Marcel Dekker, Inc., 1987.

[11] J. N. Davidson, D. A. Stone, M. P. Foster, and D. T. Gladwin, "Improved Bandwidth and Noise Resilience in Thermal Impedance Spectroscopy by Mixing PRBS Signals," *IEEE Trans. Power Electron.*, vol. 29, no. 9, pp. 4817–4828, 2014.

[12] A. J. Fairweather, M. P. Foster, and D. A. Stone, "Modelling of VRLA batteries over operational temperature range using pseudo random binary sequences," *J. Power Sources*, vol. 207, pp. 56–59, Jun. 2012.

[13] S. Nejad, D. T. Gladwin, and D. A. Stone, "A systematic review of lumped-parameter equivalent circuit models for real-time estimation of lithium-ion battery states," *J. Power Sources*, vol. 316, pp. 183–196, 2016.

[14] S. Nejad, D. T. Gladwin, and D. A. Stone, "Enhanced state-of-charge estimation for lithium-ion iron phosphate cells with flat open-circuit voltage curves," in *Industrial Electronics Society, IECON 2015 - 41st Annual Conference of the IEEE*, 2015, pp. 3187–3192.

[15] T. Barlow, S. Latham, I. Mccrae, and P. Boulter, "A reference book of driving cycles for use in the measurement of road vehicle emissions," 2009.

[16] S. Nejad, D. T. Gladwin, and D. A. Stone, "A hybrid battery parameter identification concept for lithium-ion energy storage applications," in *Industrial Electronics Society, IECON 2016-42nd Annual Conference of the IEEE*, 2016, pp. 1980–1985.

[17] S. Nejad, D. T. Gladwin, and D. A. Stone, "Sensitivity of lumped parameter battery models to constituent parallel-RC element parameterisation error," in *Industrial Electronics Society, IECON 2014 - 40th Annual Conference of the IEEE*, 2014, pp. 5660–5665.

[18] W. H. Press, *Numerical recipes 3rd edition: The art of scientific computing*. Cambridge university press, 2007.

[19] A. K. Tangirala, *Principles of System Identification: Theory and Practice*. CRC Press, 2014.

[20] W. D. T. Davies, "System identification for self-adaptive control," London, UK: Wiley-interscience, 1970, pp. 44–88.

[21] R. L. T. Hampton, "A hybrid analog-digital pseudo-random noise generator," in *Proceedings of the April 21-23, 1964, spring joint computer conference*, 1964, pp. 287–301.

[22] P. E. Wellstead, "Non-parametric methods of system identification," *Automatica*, vol. 17, no. 1, pp. 55–69, 1981.

[23] U.S. Department of Energy, "PNGV Battery Test Manual," 2001.

[24] M. J. Smith, D. T. Gladwin, and D. A. Stone, "Experimental analysis of the influence of high-frequency ripple currents on dynamic charge acceptance in lead-acid batteries," in *Industrial Electronics Society, IECON 2017-43rd Annual Conference of the IEEE*, 2017, pp. 7140–7145.

Shahab Nejad received the M.Sc. degree in Avionic Systems in 2012, and the Ph.D. degree in adaptive algorithms for battery management systems in 2016, all from the University of Sheffield, U.K. He is currently a postdoctoral researcher in the Department of Electrical and Electronic Engineering, the University of Sheffield. His research interests include large-scale energy storages and second-life applications for electric vehicle batteries.

Daniel T. Gladwin received the M.Eng. (Hons.) degree in electronic engineering and the Ph.D. degree in automated control structure design and optimization using evolutionary computing from the University of Sheffield, Sheffield, UK, in 2004 and 2009, respectively. He is a Senior Lecturer in the Department of Electrical and Electronic Engineering, the University of Sheffield, with particular interest for research into energy storage and management, power electronics, and intelligent systems.